Real Time Selective Harmonic Control—PWM Based on Artificial Neural Networks

Irati Ibanez-Hidalgo, *Graduate Student Member, IEEE*, Alain Sanchez-Ruiz, *Senior Member, IEEE*, Angel Perez-Basante, Asier Zubizarreta, Salvador Ceballos, Sergio Gil-Lopez, and Ricardo P. Aguilera, *Member, IEEE*

***Abstract*—Selective harmonic elimination-pulse width modulation (SHE-PWM) is a widely used low switching frequency modulation technique for medium-voltage high-power converters. This approach is able to adjust the converter fundamental component while eliminating low-order harmonics. However, some applications such as active power filters (APFs) require regulating simultaneously, both the fundamental and low-order harmonics in amplitude and phase. This article presents a novel selective harmonic control-PWM (SHC-PWM) modulator, valid for APFs, based on artificial neural networks (ANNs) and sequential quadratic programming (SQP). A new offline search methodology, based on a hybrid metaheuristic-numerical algorithm, is defined to calculate the solution space when both the fundamental and a low-order harmonic are controlled in phase and amplitude. The solutions obtained are used to train the ANNs offline. Afterwards, the ANN + SQP calculation method is used to solve the SHC-PWM problem in real-time (RT). Experimental results are provided for a three-level converter to verify the effectiveness of the proposed RT control method.**

***Index Terms*—Active power filter (APF), artificial neural network (ANN), metaheuristic algorithm, numerical algorithm, real-time (RT), selective harmonic control (SHC-PWM).**

Manuscript received 4 January 2023; revised 6 June 2023 and 25 August 2023; accepted 29 September 2023. Date of publication 6 October 2023; date of current version 6 December 2023. This work was supported in part by the Basque Government within the research program ELKARTEK under Grant EP4H2 (KK-2022/00039), in part by BIKAINTEK under Grant 005-B2-2020, in part by the Basque Government under Grant GIU19/292, and in part by the Australian Government through the Australian Research Council (Discovery Project) under Grant DP210101382. Recommended for publication by Associate Editor M. Ordonez. *(Corresponding author: Irati Ibanez-Hidalgo.)*

Irati Ibanez-Hidalgo is with the Tecnalia, Basque Research and Technology Alliance (BRTA), 48160 Derio, Spain, and also with the Department of Automatic Control and Systems Engineering, University of the Basque Country (UPV/EHU), 48013 Bilbao, Spain (e-mail: irati.ibanez@tecnalia.com).

Angel Perez-Basante, Salvador Ceballos, and Sergio Gil-Lopez are with the Tecnalia, Basque Research and Technology Alliance (BRTA), 48160 Derio, Spain (e-mail: angel.perez@tecnalia.com; salvador.ceballos@tecnalia.com; sergio.gil@tecnalia.com).

Alain Sanchez-Ruiz is with the Department of Electronic Technology, University of the Basque Country (UPV/EHU), 01006 Vitoria-Gasteiz, Spain (e-mail: alain.sanchez@ehu.eus).

Asier Zubizarreta is with the Department of Automatic Control and Systems Engineering, University of the Basque Country (UPV/EHU), 48013 Bilbao, Spain (e-mail: asier.zubizarreta@ehu.eus).

Ricardo P. Aguilera is with the School of Electrical and Data Engineering, University of Technology Sydney, Broadway, NSW 2007, Australia (e-mail: raguilera@ieee.org).

Color versions of one or more figures in this article are available at https://doi.org/10.1109/TPEL.2023.3322500.

Digital Object Identifier 10.1109/TPEL.2023.3322500

I. Introduction

MULTILEVEL converters are widely used for high-power medium-voltage applications due to the advantages that they present with respect to their two-level counterparts [1], [2], [3]. In these applications, low switching losses with low harmonic distortion are pursued. For this purpose, low-switching frequency modulation techniques such as selective harmonic elimination-PWM (SHE-PWM) or selective harmonic mitigation-PWM (SHM-PWM) are widely used [4], [5]. Originally, SHE-PWM was used to regulate the fundamental component while eliminating the low-order harmonics [4], [6], [7], [8], [9], [10], [11], [12], representing a suitable modulation for power applications such as motor drives, where the plant variability is low. However, in case of grid-connected applications with high plant variability like active power filters (APFs), where some current harmonics need to be generated to eliminate or minimize the harmonic content in the point of common coupling (PCC), a different approach such as selective harmonic control-PWM (SHC-PWM) is required. This modulation allows the regulation of low-order harmonics to a specific value in both amplitude and phase [13]. However, all these modulation techniques require to solve a set of nonlinear transcendental equations to obtain the set of optimal switching angles, which is not a trivial task and implies such computational cost that prevents its resolution in real-time (RT) [4].

Most of the techniques proposed in the literature to solve these equations are offline search algorithms [4] such as numerical [14], [15], algebraic [16], [17] or metaheuristic algorithms [18], [19], [20]. The solutions provided by these algorithms are usually stored in look-up tables (LUTs), which are later used in an RT controller. This implementation is suitable in case of SHE-PWM, since the optimal angles are those that provide a desired fundamental component amplitude while eliminating a set of low order harmonics. Therefore, the size of the resulting LUT is computationally affordable. However, in case of SHC-PWM, the required amplitude and phase of low-order harmonics may vary depending on the operating conditions, as it happens in case of APF applications. Thus, in this case, the size of LUT increases exponentially with the number of harmonics to be controlled, making the use of LUTs unsuitable due to the required storage capacity [8], [21].

In the case of APFs, high-switching PWM is normally used, which is not suitable for high-power applications where high

efficiency and power density are mandatory requirements. Thus, SHC-PWM is raised as a good solution for this scenario, provided that its implementation does not depend on LUTs.

In order to avoid the dependency on LUTs, some online application methods, based on algebraic algorithms or artificial neural networks (ANNs) have been proposed to calculate the firing angles in RT. In [13] and [22], a search method based on algebraic transformations and numerical search that solve the SHE-PWM problem with low computational burden was proposed. However, these techniques are not able to regulate separately the phase of every harmonic, since they are just valid for quarter-wave (QW) symmetry. On the other hand, several works based on artificial neural networks (ANNs) have also been proposed to solve the SHE-PWM in RT controllers. These approaches usually generate the training data-sets for the ANN through offline search algorithms [21], [23], [24], providing a system based on these trained ANN that is able to calculate the SHE-PWM firing angles in RT. Different versions of SHE-PWM, under constant [23] or variable [21] dc sources, are provided. Different architectures have been proposed with different types of ANNs, such as multilayer perceptron (MLP) [21], radial basis function neural network [25], generalized Hopfield neural network (GHNN) [12], or several ANNs for different ranges of the solution space [26].

All these ANN-based strategies require proper training datasets, to ensure the accurate calculation of the angles. The calculation of the datasets and the training process is carried out offline, as it requires an important computational burden. Training these ANNs is not a trivial task; and their structure will depend on the complexity of the problem. When the size of the solution space increases, a good balance between explorative and exploitative character of the search methods are required. To address this issue, some authors have proposed to combine ANNs with numerical approaches, such as Quasi-Newton [11], Levenberg-Marquardt [8], or Newton-Raphson [9]. Thus, an ANN output can be used as an initial guess for the numerical algorithm.

In all the previous works, SHE-PWM has been used to only regulate the fundamental component to a given value. To the best of the authors' knowledge, only one paper based on an ANN SHC-PWM for APFs has been presented, which simultaneously regulates the phase and amplitude of several low-order harmonics [27]. In that work, an ANN has been proposed to mitigate the harmonic content of nonlinear loads. However, this approach does not ensure the continuity of the switching angles, which could lead to overcurrents [28], since the training datasets consist of random sweeps throughout the switching angle range. In addition, the current harmonics are just mitigated and not completely eliminated. Hence, there is still an open research question that needs to be addressed before achieving a reliable use of SHC-PWM in APF applications. This article proposes a new RT ANN-based SHC-PWM method that contributes to the state-of-the-art by giving a response to the following challenges.

1) Offline calculation and analysis of the solution space, where the goal is to regulate simultaneously several harmonics.
2) Management of discontinuities in the solution space when different multidimensional sets of switching angles are required to fill the whole SHC-PWM solution space.
3) Definition of an overlap between solutions to reduce the solution transitions so the overcurrents are avoided.
4) Definition of the architecture for the ANN based modulator to enable the online estimation of the switching angles (RT execution).
5) Management of large sets of switching angles for offline ANN training.
6) Demonstration of the viability to implement the ANN SHC-PWM modulator in RT, considering a control period commonly used in high-power converters [28].

To address the above challenges, the work at hand presents an SHC-PWM implementation based on ANNs for a 3-D space formed by the fundamental harmonic amplitude (m_a) and one low-order harmonic in amplitude (m_h) and phase (ϕ_h). The proposed implementation consists of two states as follows.

1) *Offline search methodology:* The 3-D solution space is first explored using a novel offline hybrid search methodology, based on metaheuristic and classical numerical algorithms. The metaheuristic algorithm provides the explorative character while the numerical one is ideal for exploiting local information; thus, a good balance between computational burden and quality of the proposed solutions is provided. The proposed methodology provides steps to explore the solution space and some key performance indicators to calculate valid switching angles, ensuring that the obtained switching angles for two nearby operating points have continuous values and do not diverge from each other. In cases where this cannot be guaranteed, the methodology calculates additional sets of switching angles required to fill the solution space. In addition, an hysteresis overlap between these sets is provided to minimize the number of transitions between sets. Thus, this contributes to reduce overcurrents and improve the power quality and transient performance of the converter.
2) *Online SHC-PWM modulator based on ANN + Sequential Quadratic Programming (SQP):* The proposed SHC-PWM modulatoris based on ANN or ANN + SQP whenever the ANN estimation of the switching angles must be improved. Although the ANN + SQP calculation technique is executed online, the ANN (of type MLP) has been previously trained offline using the datasets obtained by the proposed search methodology. In this way, the simultaneous regulation of several harmonics through SHC-PWM can become affordable without using multidimensional LUTs. As stated before, the LUTs have some disadvantages when the number of harmonics to control increases such as higher storage requirements. In order to illustrate the approach, two different case studies are analyzed: 1) the use of a solution space covered using a single set of switching angles; and 2) a solution space where multiple sets are needed to cover the whole solution space.

The rest of this article is organized as follows. Section II briefly describes the APF concept and Section III introduces the SHC-PWM formulation used to calculate the solutions. The

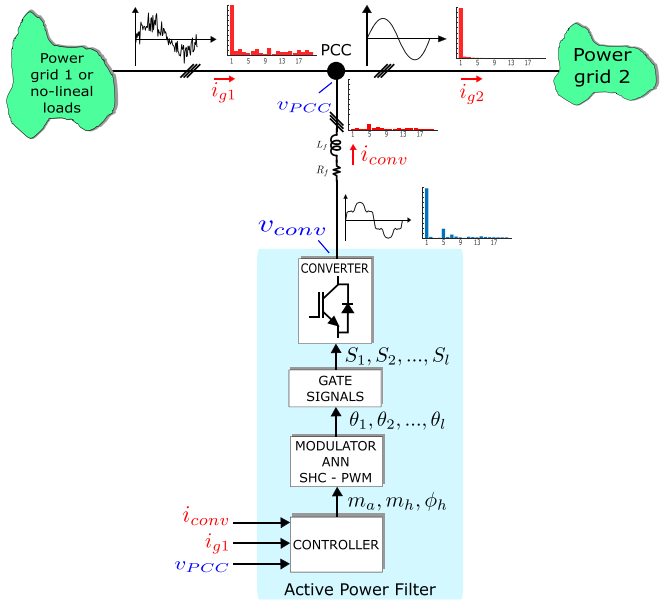

Fig. 1. APF generic block diagram.

proposed offline methodology to search the switching angles in 3-D is explained in Section IV. Section V presents the proposed ANN SHC-PWM modulator designed to be executed online for different case studies. The ANN training, executed offline, is also described in this Section. Section VI compares the proposed modulation technique to the commonly used carrier based-PWM (CB-PWM) and Section VII analyzes the scalability of the approach. Section VIII shows the obtained experimental results that validate the proposed SHC-PWM modulator. Finally, Section IX concludes the article.

II. Active Power Filter Application

An APF is used to effectively minimize (ideally eliminate) the undesirable harmonic components generated in the power grid. These harmonics appear at the grid connection point caused by other equipment connected to the grid. The minimized harmonics can be voltage or current harmonics, depending on the control mode used. In the case of minimization or compensation of current harmonics, the APF absorbs the current in the PCC to cancel out the undesired harmonic components. In Fig 1, the generic block diagram for an APF application connected in parallel is shown.

The APF is formed by a controller, a modulator, a gate signal generator, and a power converter. The focus of this article is in the modulation stage. A new ANN-based SHC-PWM modulator suitable for APF applications is presented. It takes as input the harmonic voltage references (modulation index for the fundamental (m_a) and amplitude (m_h) and phase (ϕ_h) of the controlled low-order harmonic) calculated by the controller and generated in RT the switching angles ($\theta_1, \theta_2, \ldots, \theta_l$). The proposed algorithm has been developed following a generic approach, in the sense that it can be applied to different power converter topologies, filter stages, and controller implementations.

III. SHC-PWM Formulation

Depending on the adopted waveform symmetry, the SHC-PWM technique can be formulated in three different manners: 1) QW; 2) half-wave (HW); and 3) nonsymmetry (NS) [4]. The use of QW or HW symmetry reduces the computational burden with respect to NS, as some harmonics are naturally eliminated. The QW symmetry is the most referenced one in the literature since it allows to obtain angles that will lead to a switched voltage pattern with regulated low-order harmonic amplitudes, but unregulated phase angles, as required in APF applications. On the other hand, the NS formulation can help to obtain a switched voltage pattern with regulated low-order harmonic amplitudes and phases, including dc value. In this work, as both amplitude and phase of low-order harmonics are required to be regulated, but not the dc value, a HW symmetry is adopted. Specifically, the universal formulation proposed in [7] was applied. In this formulation, the switching angles are calculated in the range $[0, 2\pi]$ (virtual switching angles) and afterwards, they are transformed to the range $[0, \pi]$ (real switching angles). In this transformation, the switching pattern, which is not initially predefined, is directly obtained. Moreover, as a three-phase system is used, only nontriplen odd harmonics are considered.

The equations for the output voltage waveform, the a_h and b_h coefficients, and the normalized harmonic amplitude (m_h) and phase (ϕ_h) of each harmonic are calculated as

$$v_{a0} = \sum_{h=1,3,5,7,\ldots}^{\infty} a_h \cos(h\omega t) + \sum_{h=1,3,5,7,\ldots}^{\infty} b_h \sin(h\omega t) \quad (1)$$

$$a_h = -\frac{2V_{dc}}{(L-1)h\pi} \sum_{k=1}^{2l} \sin(h\theta_{k,v}) \quad (2)$$

$$b_h = \frac{2V_{dc}}{(L-1)h\pi} \sum_{k=1}^{2l} \cos(h\theta_{k,v}) \quad (3)$$

$$m_h = 2\frac{\sqrt{a_h^2 + b_h^2}}{V_{dc}} \quad (4)$$

$$\phi_h = \begin{cases} \arctan\left(\frac{b_h}{a_h}\right) - \pi & b_h < 0,\ a_h < 0 \\ \arctan\left(\frac{b_h}{a_h}\right) + \pi & b_h > 0,\ a_h < 0 \\ \arctan\left(\frac{b_h}{a_h}\right) & b_h < 0,\ a_h > 0\ \&\ b_h > 0,\ a_h > 0 \end{cases} \quad (5)$$

where V_{dc} is the total dc bus voltage, L is the number of levels of the converter, l is the number of switching angles to calculate, h is the harmonic identifier, and $\theta_{k,v}$ is the identifier for every virtual switching angle.

The cost function (CF) which should be minimized by the search algorithm to calculate the set of switching angles from the aforementioned equation is defined as

$$CF = \varepsilon_{a1}^2 + \varepsilon_{b1}^2 + \varepsilon_{a5}^2 + \varepsilon_{b5}^2 + \cdots + \varepsilon_{ah}^2 + \varepsilon_{bh}^2 + f_{valid}. \quad (6)$$

ε_{ah} and ε_{bh} represent the error for every regulated harmonic and f_{valid} is a penalty function that evaluates the validity of the

obtained switching angles. This function verifies that the next constraints are fulfilled [7].

1) The obtained virtual switching angles must be inside the range $[0, 2\pi]$.
2) The number of levels of the output voltage waveform cannot exceed the number of levels of the converter.
3) The real switching angles must keep a predefined minimum distance between them. In this way, the minimum conduction time of the converter switches can be assured. This time is the sum of the dead time and the minimum on time of the switch.

If any of these constraints is not fulfilled, the f_{valid} will return a value higher than the convergence threshold so the CF final value is high and the solution is discarded by the search algorithm. On the contrary, if all the constraints are satisfied, f_{valid} will return a 0 and the CF final value will be calculated only with ε_{ah} and ε_{bh} coefficients.

IV. Proposed Offline Search Methodology for 3-D Solution Space

In this section, the offline search methodology used to calculate the SHC-PWM solution space is explained. In particular, 3-D have been considered, regulating accurately the amplitude of the fundamental harmonic and the amplitude and phase of another low-order harmonic. However, the proposed methodology is scalable to a higher number of dimensions (higher number of harmonics to be regulated simultaneously). To the authors' knowledge, this is the first time that an analysis of the whole solution space for the SHC-PWM formulation, where at least one low-order harmonic is regulated in amplitude and phase.

The methodology uses a metaheuristic algorithm, benefiting from its exploration ability, to find the switching angles, which is hybridized with a numerical method for exploiting local information and thus improving the accuracy. A hybrid algorithm that combines a genetic algorithm (GA) with a gradient descent (GD) strategy, named GA-GD, has been selected following the method presented in [20]. The hybridization consists of the execution of the GD strategy after certain number of generations, trying to explode the information accumulated by the GA. In this way, faster convergence and lower computational burden are achieved while accuracy is improved.

When applying the SHC-PWM formulation to regulate several harmonics, not all the calculated set of switching angles are suitable. Certain constraints should be imposed to improve the robustness of the solution as follows.

1) First, the obtained switching angles within a set have to ensure continuity in all the dimensions of the solution space. Otherwise, relevant transient overcurrents may be generated due to discontinuities in the solutions [28].
2) Additionally, due to its complexity, multidimensional solutions spaces could require several sets of switching angles to be completely filled, leading to some transitions between different sets that cannot be avoided, providing discontinuities. To minimize the number of transitions, the sets of switching angles should be as large as possible and overlaps between different sets should be guaranteed to avoid unnecessary transitions from one set to another in the border regions. These facts are very relevant, since converter overcurrents can be minimized when the number of transitions is limited [28].
3) Besides, the real switching angles in the range [0,π] must have a minimum distance between them. Additionally, this minimum distance provides the required minimum on time of the semiconductors [29].
4) Finally, the variation of switching angle values between close operating points must be limited. In this way, the performance of high-level closed loop controls is improved.

The offline methodology proposed in this article analyzes the solution space for 3-D while taking into account these constraints. The steps of the proposed methodology (see Fig. 2) to calculate the firing angles throughout the SHC-PWM solution space are the following:

A. STEP 1: Search and Selection of Solutions in 1-D

In this step, the switching angles for the classical SHE-PWM technique are calculated in 1-D (m_a). The calculated switching angles allow to regulate m_a and eliminate the rest of the considered lower-order harmonics. The switching angles are obtained using the GA-GD hybrid algorithm.

The GA-GD is run several times with different randomized initial populations, so different sets of switching angles are obtained. In Fig. 3, an example of a set of switching angles for a three-level (3 L) converter, when m_a is regulated and the 5th, 7th, 11th, and 13th harmonics are eliminated using HW symmetry and 12 switching angles is depicted. The GA-GD is able to provide more than one set of switching angles, as it is an initial population based algorithm. The valid sets are postprocessed to determine the optimal solutions. Besides the previously commented constraints, the following specifications must be satisfied.

1) The set of switching angles must provide a solution in the range of m_a that is required to be controlled by the grid-connected application. If the set does not have any solution in the desired m_a range, it is not considered as a valid solution. In the case of grid-connected applications, high values of m_a are required to be controlled (see Fig. 3).
2) The switching angles must be as equidistant as possible with each other at each m_a, in order to ensure that the distribution of the switching instants resembles that of the CB-PWM, as a way to improve the dynamic performance of the power converter control. This distance is set empirically. There is not a specific number which is considered to be the optimum one. It may depend on the number of angles, the harmonics to be controlled and eliminated, or the number of converter levels. In this work, the standard deviation of all distances has been selected to be equal or lower than $0.7\frac{\pi}{n^o angles}$.
3) $\Delta\theta_k/\Delta m_a$ for every switching angle, considering $\Delta m_a = 0.1$, cannot be higher than a threshold (0.25 rd). This contributes to improve the robustness of the proposed method as it assures that variations in the m_a value have a

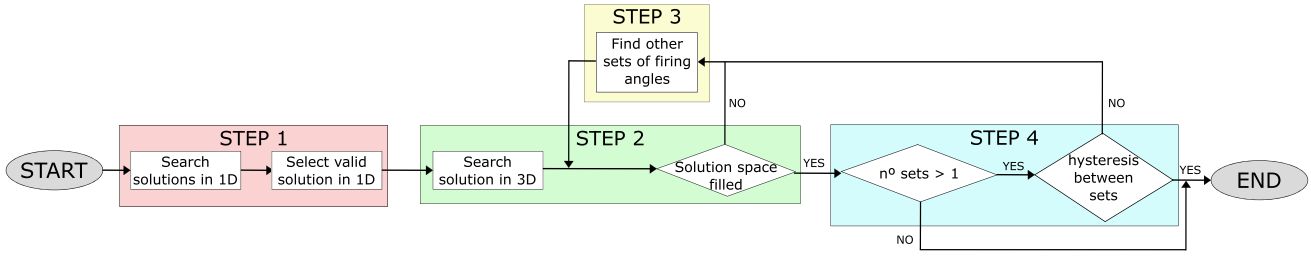

Fig. 2. Flowchart of the proposed methodology.

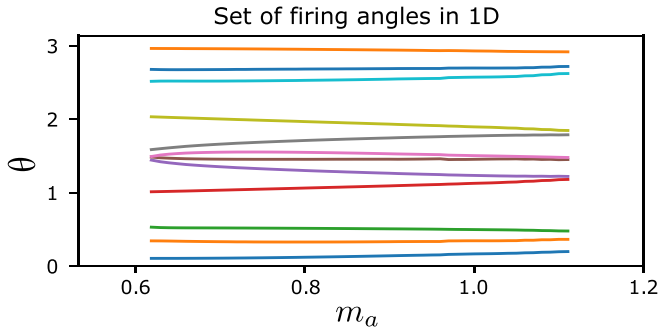

Fig. 3. SHE-PWM optimal set of real switching angles in 1-D with HW symmetry.

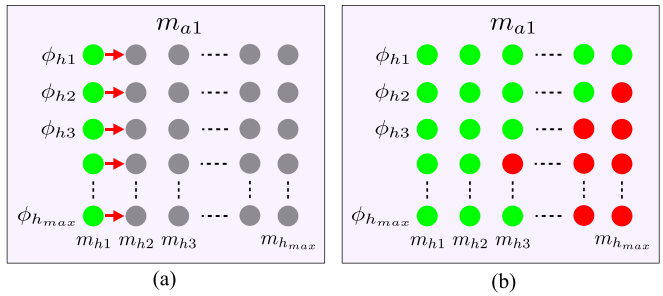

Fig. 4. (a) Way of searching for 3-D. (b) Example of final result.

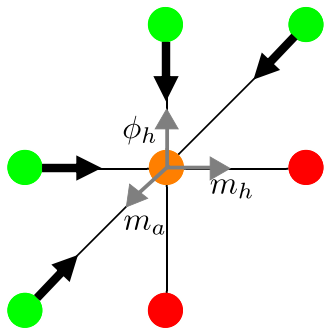

Fig. 5. Directions to fill empty points.

low effect on the control and the obtained switching angles resemble the ones of the CB-PWM.

If the set of switching angles does not fulfill one of the previously mentioned requirements, it is considered to be an invalid solution. The sets of firing angles considered valid are used to calculate the solution space for the SHC-PWM in 3-D.

B. STEP 2: Search of Solutions in 3-D

On the basis of the valid 1-D (m_a) solutions calculated in the STEP 1, the solution space is searched and extended to consider the rest of the dimensions (harmonic amplitude (m_h) and phase (ϕ_h)). The objective is to obtain a set of switching angles as large as possible. Thus, a larger area of the solution space is covered.

For that purpose, the SQP numeric method [30] is used to find the switching angles, due to its fast convergence, local search methodology departing from a good initial guess and its ability to constrain the minimum distance between switching angles. Hence, for every 1-D solution obtained in the first step, the associated 3-D solution is calculated through the search procedure depicted in Fig. 4(a). For simplicity, for a predefined m_a, a 2-D space is represented. The gray circles represent the (m_a, m_h, ϕ_h) combinations for which the switching angles have not been calculated yet. The green ones are those with valid switching angles and the arrows represent the direction to search new switching angles. Initially, it is considered that for each m_a, all the combinations with $m_h = 0$ have the same switching angles for all the possible ϕ_h values; specifically, the switching angles calculated in the STEP 1 for that specific m_a. Next, using these solutions as initial guess for the SQP algorithm, the switching angles throughout the m_h range for each (m_a, ϕ_h) combination are calculated. Additionally, $\Delta\theta_k/\Delta m_a$, $\Delta\theta_k/\Delta m_h$, and $\Delta\theta_k/\Delta\phi_h$ are checked for all the operating points to ensure that the constraints imposed in STEP 1 for 1-D are also satisfied in the 3-D space. Hence, if a set of switching angles provides a CF value under a defined threshold [29] and $\Delta\theta_k/\Delta m_a$, $\Delta\theta_k/\Delta m_h$, and $\Delta\theta_k/\Delta\phi_h$ are lower than a specific value (0.25 rd), this set is considered as a valid solution and added to the solution space in 3-D. The process is repeated iteratively, trying to fill the whole 3-D solution space. However, at the end of the process, some operating points might not have a valid solution [red circles in Fig. 4(b)].

To cope with these points, the following procedure to prolong as much as possible the set of switching angles with the desired properties is applied. Each point in the 3-D solution space has six close points around, two per dimension. Hence, this set of surrounding points of a given (m_a, m_5, ϕ_h) combination to be calculated is used as initial guess for the SQP algorithm. This is represented in Fig. 5, where the orange circle represents the

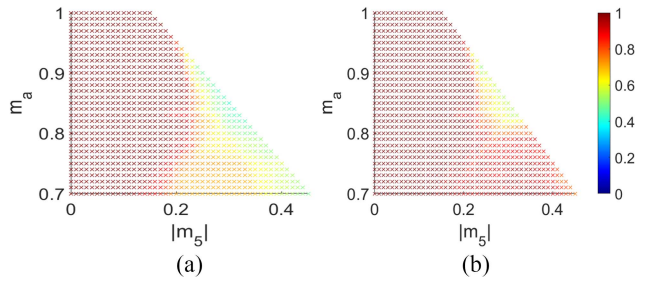

Fig. 6. Percentage of filled phases for each (m_a, m_h) combination for $h = 5$. (a) Before set prolongation. (b) After set prolongation.

empty point to be filled, the green circles are points with valid solutions, and the red ones are points for which a valid solution has not been found yet. For this specific case, the SQP is executed four times, using every green point as initial guess. The obtained four solutions are evaluated to verify the constraints imposed in the CF ($CF < 10^{-5}$) [29] and in the switching angles, i.e., $\Delta\theta_k/\Delta m_a$, $\Delta\theta_k/\Delta m_h$, and $\Delta\theta_k/\Delta\phi_h$. Note that more than one solution can satisfy these criteria. Thus, the solution with lower value in (6) is selected for the objective operating point (orange). Following this procedure and on the basis of the 1-D solution depicted in Fig. 3, for $h = 5$ the percentage of ϕ_5 filled for each (m_a, m_5) combination can be increased significantly, as seen in Fig. 6(a)–(b).

If at the end of this process the obtained set of switching angles covers the required solution space, the proposed methodology jumps directly to STEP 4, detailed in Section IV-D; where, if more than one 3-D set of switching angles exist, the hysteresis between them is checked. Otherwise, the STEP 3 explained in Section IV-C is carried out, where another 3-D set of switching angles is calculated to try to fill the full solution space.

C. STEP 3: Completing the Solution Space With Other 3-D Sets of Solutions

If the set of switching angles obtained in the STEP 2 does not complete the desired (m_a, m_h, ϕ_h) 3-D solution space, other angle sets must be calculated to fill the empty space.

For this purpose, the following strategy is adopted. Among the points without a solution, one is randomly selected in which the hybrid algorithm GA-GD detailed in the beginning of Section IV is applied. In order to obtain different solutions, the GA-GD is executed ten times, from which only the ones satisfying the (6) threshold are considered. Each of the valid solutions are used as initial guess for the SQP algorithm to calculate new 3-D sets of switching angles. These sets are calculated following the next stages (Fig. 7).

1) The initial point to start the calculation of the new set of switching angles is represented with a black circle in Fig. 7(a). From this point, for this specific (m_a, ϕ_h) combination, solutions throughout the m_h range are calculated using the SQP algorithm. As it has been previously mentioned, only the solutions satisfying the constraints in CF, $\Delta\theta_k/\Delta m_a$, $\Delta\theta_k/\Delta m_h$, and $\Delta\theta_k/\Delta\phi_h$ are considered as valid.

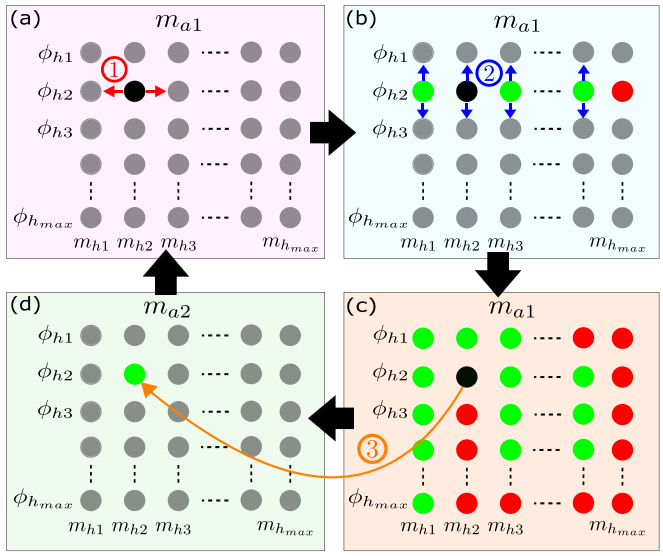

Fig. 7. Stages to find other 3-D sets of switching angles. (a) Search for solutions throughout m_h range for a combination of (m_a, ϕ_h). (b) Search for solutions throughout ϕ_h range for a specific m_a and all available m_h. (c) Obtained solution space in 2-Ds for a specific m_a. (d) Finding solution for the next m_a.

2) Once these solutions have been obtained, they are used as initial points for the SQP to calculate the solutions for all the ϕ_h range [Fig. 7(b)]. In this way, the solution space for all (m_h, ϕ_h) combinations for a specific m_a is obtained [Fig. 7(c)].
3) At this point, using the switching angles obtained initially with the GA-GD as initial guess, the solution for the next closest m_a for the specific (m_h, ϕ_h) is calculated [Fig. 7(d)].
4) Once this solution has been calculated, the previous three stages are executed again throughout the m_a range until the full 3-D solution space is filled.

These four stages are carried out for each of the initial points calculated by the GA-GD. Thus, different 3-D sets of switching angles are calculated. From all the obtained sets, the one filling more empty area of the solution space is selected. If more than one 3-D set of switching angles fill the same amount of empty points in the solution space (the empty operating points not filled by the original 3-D set given by STEP 2), the largest set considering all its filled operating points is selected. Finally, a check is carried out to evaluate if the calculated sets of switching angles cover the whole desired 3-D solution space. If not, the process detailed in this subsection is repeated (stages 1, 2, 3, and 4), generating more switching angle 3-D sets until the whole solution space is filled.

D. STEP 4: Check Hysteresis Between the Sets of Switching Angles

When more than one set of switching angles is required to cover the solution space, it is essential to avoid unnecessary transitions between sets. These transitions are due to the ripple of the reference voltage given by the control loop, caused by the low

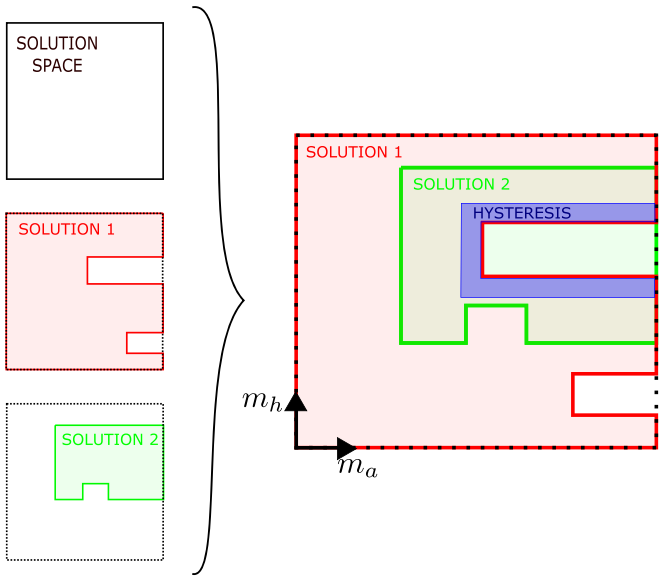

Fig. 8. Hysteresis between solutions for a defined ϕ_h.

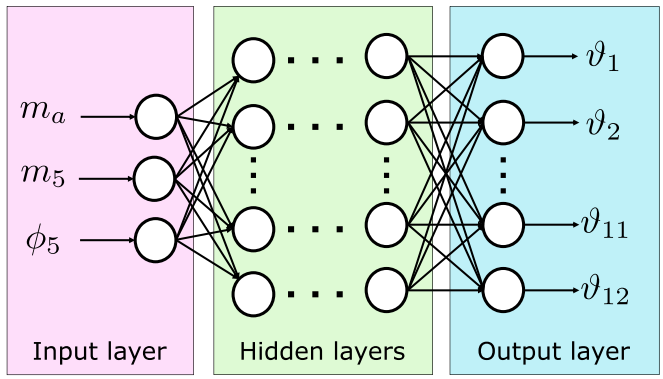

Fig. 9. ANN architecture.

TABLE I
SOLUTION SPACE CONSIDERED FOR BOTH CASE STUDIES

Magnitude	Case 1 range	Case 2 range	Step size
m_a	[0.7, 1.0]	[0.7, 1.0]	0.01pu
m_5	[0, 0.12]	[0, 1.15-m_a]	0.01pu
ϕ_5	[-π, π]	[-π, π]	$\frac{\pi}{50} rad$

control and switching frequencies in high-power converters [28]. To avoid them, an hysteresis band among the sets that overlaps the different solutions is required and needs to be verified. The hysteresis value is set to the double of the control ripple and is checked in both m_a and m_h dimensions considering the conditions in [29]. This hysteresis band is represented in blue in Fig. 8, where the hysteresis is verified for a defined ϕ_h between two different solutions. This check reduces the number of transitions between sets in RT applications, avoiding the overcurrents induced by transitions [28]. In case the hysteresis is not satisfied, another set of switching angles should be obtained following the stages of the STEP 3. Otherwise, the desired 3-D solution space is completed and the search process is over.

V. Online Implementation of SHC-PWM: Case Studies

This section details the online implementation of SHC-PWM based on ANNs and SQP for RT applications, considering two case studies with different complexity.

The proposed methodology has been used to obtain offline the switching angles of a solution space that allows to regulate m_a, the 5th harmonic in amplitude (m_5) and phase (ϕ_5), and eliminates the low-order harmonics 7th, 11th, and 13th for a 3 L converter. Solutions with HW symmetry and 12 switching angles in the first HW have been calculated. Solutions with just ten switching angles could be employed. However, these sets present a high number of discontinuities and feasible solutions to fill the whole solution space were not found. In this way, two additional switching angles provide the required degree of freedom to obtain a feasible solution space. For this study, the value set for the maximum equidistance standard deviation is set to 0.183 rd and the minimum distance between the switching angles is set to 0.0061 rd.

In order to implement the mapping from the 3-D solution space (m_a, m_5, ϕ_5) to the 12 switching angles corresponding to each point, a set of ANNs have been trained offline. ANNs are known for their adaptability and generalization capacity to infer causal relationships in nonlinear problems that have a complex nature [31]. Between all the types of ANNs, the multilayer perceptron (MLP) ANN has been chosen, which is considered to be well suited for this problem because of its vector to vector nature [10]. This ANN consists of one input layer which will receive the desired m_a, m_5, and ϕ_5 as inputs, a number of variable hidden layers depending on the complexity of the problem at hand, and an output layer that provides the required 12 switching angles as represented in Fig. 9.

In an ANN, each layer consists of p number of neurons, whose output is given by

$$y(k) = f\left(\sum_{j=1}^{p} W_j x_j(k) + b\right) \tag{7}$$

where x is the input of the neuron, W is the weight of the input, b is the bias, p is the number of neurons in the previous layer, and f is the activation function used at each layer [31]. The MLP is trained to adjust the W and b parameters to ensure that the trained outputs fit the desired ones for a specific set of inputs. This training stage is carried out by a gradient descent (or variations) methodology.

Two different case studies have been considered: 1) a solution space that is covered using a single set of switching angles; and 2) a solution space where seven different sets of switching angles are needed to cover it. For every case study, the considered range for each dimension (m_a, m_5, ϕ_5) and the step size between consecutive operating points in the solution space is included in Table I. In addition, since an ANN introduces an approximation error, the (6) threshold that assesses the validity of the predicted switching angles has been set to 10^{-4} [29].

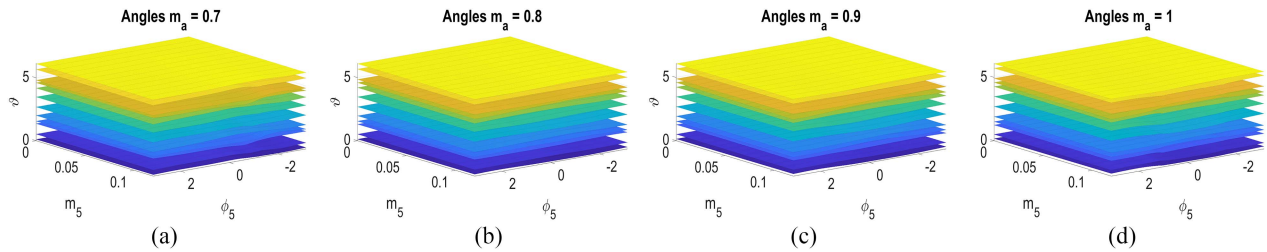

Fig. 10. Example of a set of switching angles for the first case study with $h = 5$. (a) $m_a = 0.7$. (b) $m_a = 0.8$. (c) $m_a = 0.9$. (d) $m_a = 1.0$.

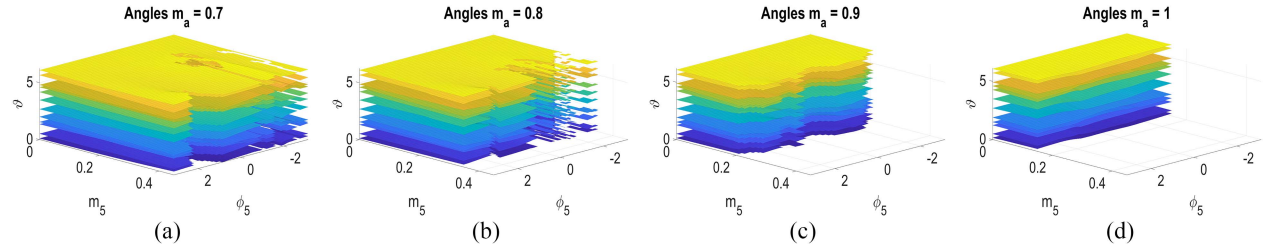

Fig. 11. Example of a set of switching angles for the second case study with $h = 5$. (a) $m_a = 0.7$. (b) $m_a = 0.8$. (c) $m_a = 0.9$. (d) $m_a = 1.0$.

A. *Online SHC-PWM Case 1: Single Set of Switching Angles*

This case study considers a solution space (Table I) which is completely covered by a single set of switching angles (Fig. 10), guaranteeing the continuity in all the solution space. Therefore, only one ANN is trained for its implementation in RT. An ANN architecture (layers, neurons, and activation functions) comparison has been implemented to improve the ANN design. As a result of this study, which is done offline, the ANN is composed by two hidden layers containing 50 neurons each. Moreover, the activation functions have been set to "relu" and "sigmoid" for the hidden layers and "linear" for the output layer, trying to guarantee the output sensitivity.

For grid-connected applications, it is required that RT solutions are obtained for the whole range of modulation indexes, harmonic amplitudes, and phases. Otherwise, if nonvalid solutions were calculated by the ANN, the grid-connected converter might experience overcurrent and then be disconnected. As a consequence, an ANN able to have a 100% of prediction success for the switching angles is required. Since the allowed error in (6) is very low (10^{-4}) and the success rate is high (100%), the step magnitude at every dimension has been selected very small (see Table I). The ANN has been trained with a modified Adam methodology for 20 000 epochs using the whole set of switching angles as training data and without considering a validation set.

B. *Online SHC-PWM Case 2: Multiple Sets of Switching Angles*

This case study considers a solution space that requires several sets of switching angles to be completely covered. An example of one of these sets is depicted in Fig. 11. The range of the magnitudes of the solution space are depicted in Table I. It can be noticed that the maximum value for m_5 depends on the value of the fundamental component, and is calculated as

$$m_{5,\max} = 1.15 - m_a. \tag{8}$$

This means that the SHC-PWM modulator has been designed to provide the same level of applicability than CB-PWM modulation technique with injection of the 3rd harmonic, which is commonly employed in APFs. To make them equivalent, the sum of the fundamental harmonic amplitude and the controlled harmonic amplitudes for SHC-PWM is considered not to be higher than 1.15 p.u., which is the maximum affordable value without overmodulation when a 3rd harmonic is injected in the CB-PWM. Hence, based on (8), the range of the 5th harmonic amplitude for each value of m_a is defined from 0 to $m_{5,\max}$. To cover this solution space, seven different sets of switching angles have been calculated.

As seven sets of switching angles exist, a different ANN (called switching angle ANN (SA-ANN)) for every switching angles set is trained, trying to infer the specificity of each set while guaranteeing their desired properties. In order to determine the architecture of each SA-ANN, a comparative analysis has been carried out, considering different SA-ANN architectures (neurons and layers). In this case, for all the hidden layers, the "sigmoid" activation function has been used.

As an example, Table II shows, for the first set of switching angles, the percentage of valid approximations (see Section III) obtained by different SA-ANN architectures. It can be seen that due to the complexity of the solution space, even using a high number of hidden layers and neurons, it is not possible to fulfill the (6) threshold for all the operating points considered for the SA-ANN. In order to address this issue, a hybrid approach has been implemented, where the switching angles provided by the SA-ANN are used as initial guess for the SQP numerical algorithm. Using this procedure for the considered seven sets,

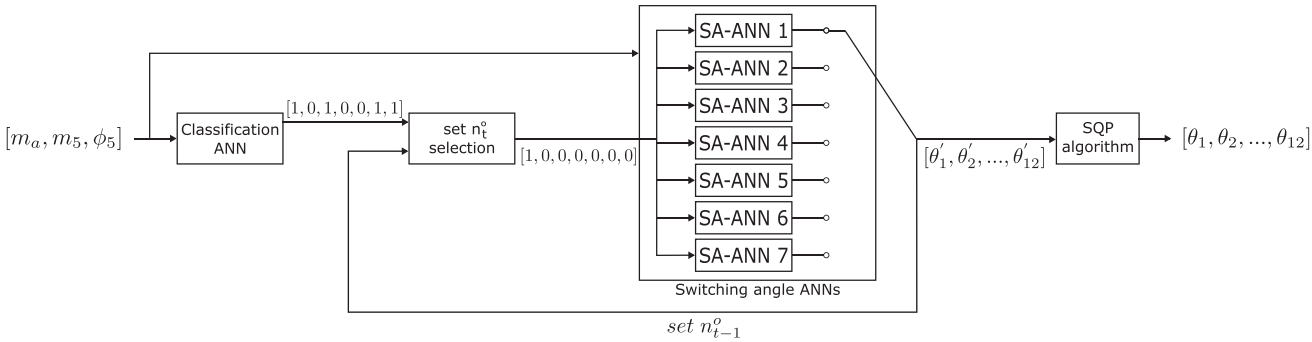

Fig. 12. Schema of online SHC-PWM for the second case study.

TABLE II
PERCENTAGE OF VALID SOLUTIONS FOR THE FIRST SET OF SWITCHING ANGLES IN THE SECOND CASE STUDY

Nº hidden layers	Size of hidden layers	% of valid predictions
2	50-50	57.44%
2	60-60	59.38%
3	30-30-30	63.07%
3	40-40-40	74.80%
4	30-30-30-30	77.15%
4	40-40-40-40	83.58%
6	50-50-50-50-50-50	91.57%

TABLE III
OPTIMAL SA-ANN STRUCTURES FOR THE SECOND CASE STUDY

Nº of set	Nº of hidden layers	Size of hidden layers	Nº of training points
1	4	40-40-40-40	91893
2	4	40-40-40-40	42099
3	4	30-30-30-30	69230
4	4	30-30-30-30	73907
5	4	40-40-40-40	13449
6	4	40-40-40-40	3596
7	3	30-30-30	3907

all operating points in the solution space fulfill the CF threshold constraint. The obtained optimal SA-ANN structure for each set of switching angles is depicted in Table III. Note that as the approach is intended to be applied in RT applications, the selected SA-ANN structure has been the one that provides the best initial guess with minimum SA-ANN size, with the aim of reducing the computational cost.

As the solution space is divided into different switching angle sets, an approach is required to select which set of switching angles (and thus, SA-ANN) is required to be executed for every operating point. In this work, an additional classification ANN is proposed to determine which SA-ANN may be used at every operating point in the RT execution.

The operating points, given by the (m_a, m_5, ϕ_5) combinations, are the inputs of the classification ANN, which provides seven binary outputs determining which SA-ANNs can be executed for each operating point. After an optimization process, the architecture for the classification ANN consists of four hidden layers of 80 neurons each and a "sigmoid" activation function for all the layers, including the output layer.

The execution diagram of this case study is represented in Fig. 12, where there is a selector which provides the specific SA-ANN to be executed among the valid SA-ANNs given by the classification ANN for a specific operating point. The selector performance is based on some criteria. The first criterion is to keep executing the same SA-ANN as in the previous control cycle if this SA-ANN is still valid for the new operating point. However, if this SA-ANN is no longer valid, among the other possible valid SA-ANNs, the one which represents the largest solution is chosen (see Table III). In this way, the number of transitions between sets of switching angles is reduced. Once the selected SA-ANN has been chosen, the initial switching angles are estimated (θ'_k), which are used as initial guess for the SQP method, in case they are required to be optimized. Finally, the SQP method is executed, obtaining the final switching angles (θ_k). For a high number of iterations and evaluations of the SQP, better results are obtained. However, it implies an increase in the execution time. Therefore, in this work, the number of iterations and evaluations has been limited.

Finally, since the classification ANN cannot generate erroneous data, because an error could activate a SA-ANN that has not been trained for a specific operating point, leading to invalid switching angles at the output, the classification ANN is also trained to achieve a prediction accuracy of 100%. In Fig. 13, an example of the firing angles predicted by the SA-ANN + SQP are depicted together with the ideal firing angles calculated offline. In Fig. 13(a), the 5th harmonic is controlled to zero, while in Fig. 13(b) the amplitude of the fundamental and the phase of the 5th harmonic are fixed to $m_a = 0.71$ and $\phi_5 = \pi$, respectively. A good agreement between the ideal switching angles and those calculated online in real time by the proposed SA-ANN + SPQ is observed.

VI. COMPARISON WITH EXISTING MODULATION TECHNIQUES

To the best of authors' knowledge, this is the first time that an SHC-PWM is implemented to control simultaneously the amplitude and phase of several harmonics. As it has been detailed in Section I, previous works related to low switching

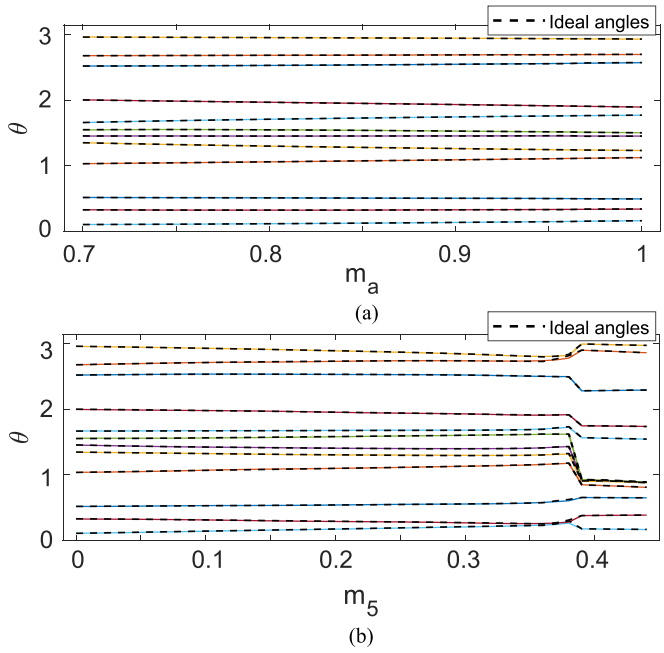

Fig. 13. Comparison of ideal and ANN firing angles. (a) Variable m_a, $m_5 = 0$, $\phi_5 = 0$. (b) $m_a = 0.71$, variable m_5, $\phi_5 = \pi$.

frequency modulations just mitigate the harmonics [27], instead of controlling them accurately; or just control the amplitude, instead of amplitude and phase [13], [22]. Therefore, they are not suitable for applications such as active filtering where it is required to accurately control the amplitude and phase of several harmonics. As there is not a comparable real-time SHC-PWM in the technical literature, a benchmark of the proposed technique versus to a more conventional real-time modulation technique, such as CB-PWM, has been carried out.

In Fig. 14, the output voltage waveform of a 3 L converter together with its associated harmonic spectrum provided by CB-PWM and SHC-PWM under equal effective switching frequency (600 Hz) for a specific operating point ($m_a = 0.8$, $m_5 = 0.2$, $\phi_5 = 0$) are depicted. The triplen harmonics, which are naturally cancelled in three-phase systems, are marked in red and the controlled harmonics in green. As it can be noticed, under such low switching frequency, the CB-PWM, unlike SHC-PWM, is not able to control properly the low order harmonics, highlighting the contribution of the proposed SHC-PWM modulator. In order to control precisely the harmonics with the CB-PWM, the switching frequency must be increased, increasing the switching losses. This is not suitable for high-power medium-voltage applications, where low switching losses are required.

VII. Scalability

One of the main benefits of the proposed ANN-based SHC-PWM modulator over modulators based on LUTs is its scalability.

The size of ANNs, unlike LUTs, does not increase exponentially with the number of controlled harmonics. In order to emphasize this feature, a study has been carried out comparing the storage capacity needed to control a different number of harmonics as depicted in Table IV. The value range considered in this study for every controlled harmonic is included in Table V. In all the cases, the solution space is covered using a single set of firing angles; hence, a single SA-ANN is required. Note that when only the fundamental harmonic is controlled (H_1), as there is no need to control the phase of any harmonic, a QW symmetry with five firing angles is used. When the 5th (H_5) or 7th (H_7) harmonics are controlled, the phase is also regulated. Therefore, HW symmetry with 12 firing angles is used. Each switching angle value (data point) requires 16 bits to be stored in memory.

TABLE IV
Storage Capacity for a Different Number of Controlled Harmonics

Controlled harmonics	Eliminated harmonics	Nº data	LUT memory	SA-ANN size	SA-ANN memory
H1	H5, H7, H11, H13	31	310B	2L100	23kB
H1, H5	H7, H11, H13	40703	976.8kB	2L50	6.5kB
H1, H5, H7	H11, H13	6609141	158MB	6L80	67.7kB

TABLE V
Solution Space Considered for the 1st, 5th and 7th Harmonics

Magnitude	Range	Step size
m_a	[0.7, 0.9]	0.01pu
m_5,m_7	[0, 0.1]	0.01pu
ϕ_5,ϕ_7	$[-\pi, \pi]$	$\frac{\pi}{25} rad$

In Table IV, it can be observed that when a single harmonic is controlled, the required memory size of the LUT is much smaller than the one needed by the SA-ANN, making the SA-ANN not useful for a single dimension. However, as the number of controlled harmonics increases, the required memory size to store the switching angles in a LUT increases exponentially, making this solution difficult to extrapolate to case studies with several harmonics. Instead, the increment of the required storage memory for the SA-ANN is significantly lower, as the size of the SA-ANNs do not increase exponentially. Consequently, it can be concluded that, when the number of controlled harmonics increases, the ANNs are a more implementable approach than the LUTs.

VIII. Experimental Results

In this section, the experimental results for the two case studies presented in Section V are detailed and analyzed. The experimental setup used to obtain the results is shown in Fig. 15. The main goal of these results is to prove the viability to implement the proposed SHC-PWM modulator in RT. The results have been obtained for a 3 L converter where the fundamental and the 5th harmonic are regulated and the 7th, 11th, and 13th harmonics are eliminated. The ANNs associated to each of the case studies have been trained offline using the open source KERAS library, and then exported to MATLAB/Simulink in order to be implemented in a RT control system; specifically, a Speedgoat RT target machine (Intel Core i7, 4.2 GHz Quad Core CPU, and 32 GB RAM). The selected target, besides the CPU, also contains a

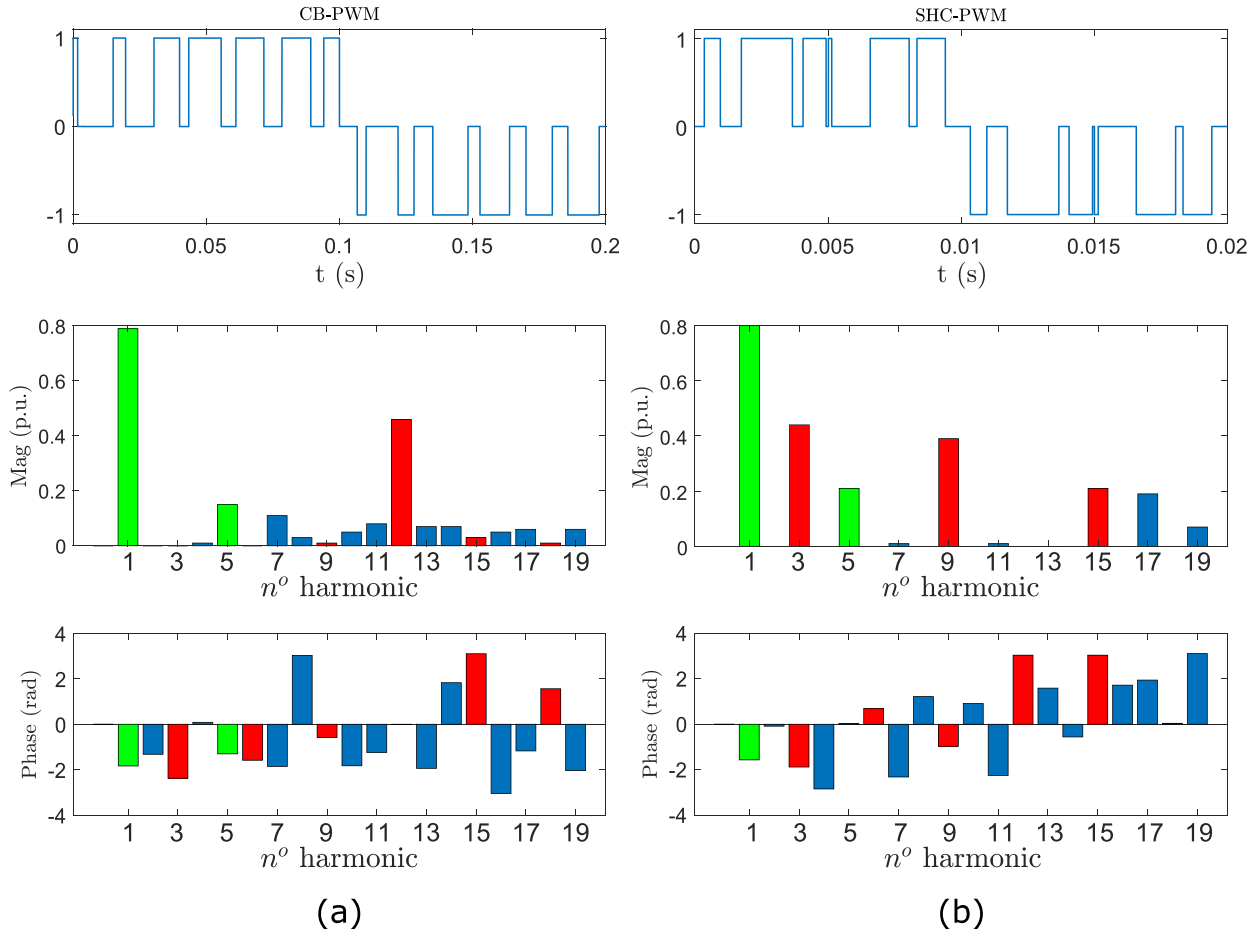

Fig. 14. Comparison of CB-PWM and SHC-PWM under same conditions. (a) CB-PWM waveform and FFT. (b) SHC-PWM waveform and FFT.

Fig. 15. Experimental setup.

FPGA block. In this way, the code execution is shared among the CPU and the FPGA. The CPU handles the calculation of the switching angles depending on the operating point by means of the different trained ANNs, the implemented selector, and the SQP (if required) with an execution step of $500\,\mu$s. Through the calculated angles, three phase switching states and their corresponding switching times, for the next control period are obtained. The FPGA, on the other hand, receives the switching states and switching times and calculates the semiconductor gate signals for a 3 L converter, with an execution step of 10 ns.

In order to demonstrate the suitability of the proposed modulator, the calculated gate orders are reconstructed obtaining the voltage waveforms. Next, an analysis of the waveforms and the time requirements is carried out.

A. *Voltage Waveform Analysis*

In Figs. 16(a) and 17(a), the voltage waveforms obtained for the first and second case studies, respectively, are depicted. For each case study, three different (m_a, m_5, ϕ_5) operating points have been evaluated. It is observed that for different operating points of the solution space, the obtained voltage waveforms always contain three levels and 12 switching angles with HW symmetry. Moreover, transitions between different operating points are properly performed in RT without incurring in undesired delays on the calculation of the solutions or distortion in the waveforms. In Fig. 17(a), the set of switching angles, $set\ n^o$, used for each operating point is represented with a green line. For each operating point, a different set of switching angles has been evaluated.

Additionally, the firing angles for each operation point are depicted in Figs. 16(b) and 17(b) for the first and second case study, respectively.

A sweep in each dimension for each case study has been realized. Each sweep has been done covering the whole range of the solution space for the specific dimension (Table I). As a

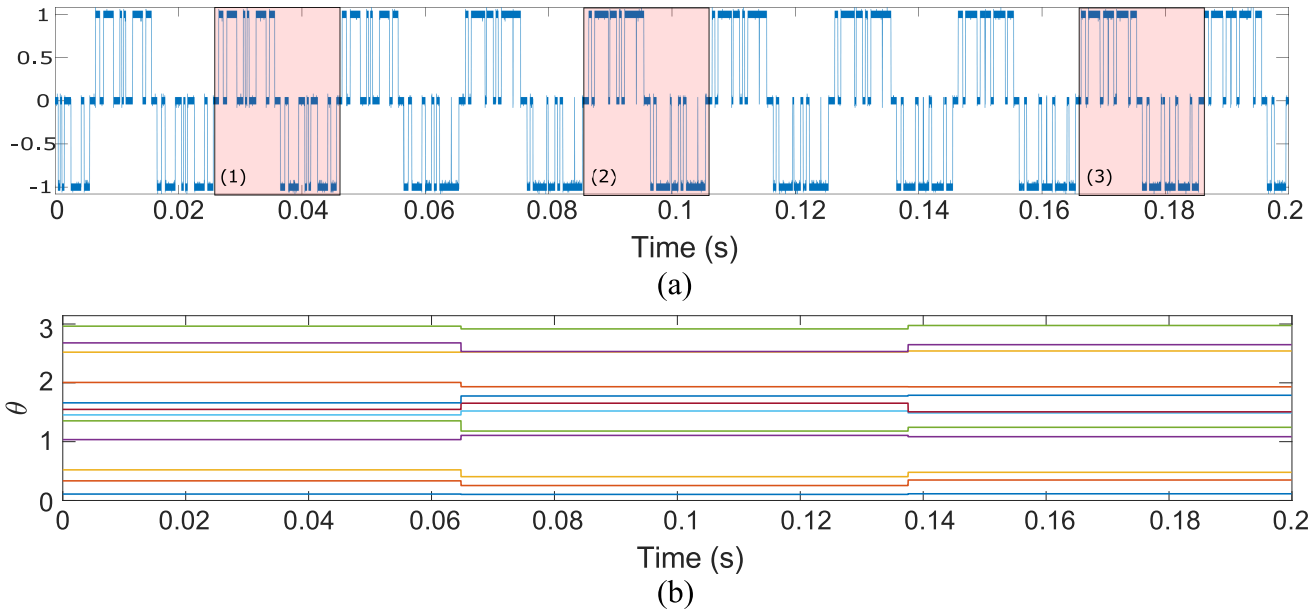

Fig. 16. (a) V_{a0} waveform for first case study. (1) $m_a = 0.7$, $m_5 = 0$, $\phi_5 = 0$. (2) $m_a = 1$, $m_5 = 0.12$, $\phi_5 = 0$. (3) $m_a = 1$, $m_5 = 0.12$, $\phi_5 = -\frac{\pi}{2}$. (b) Firing angles for first case study.

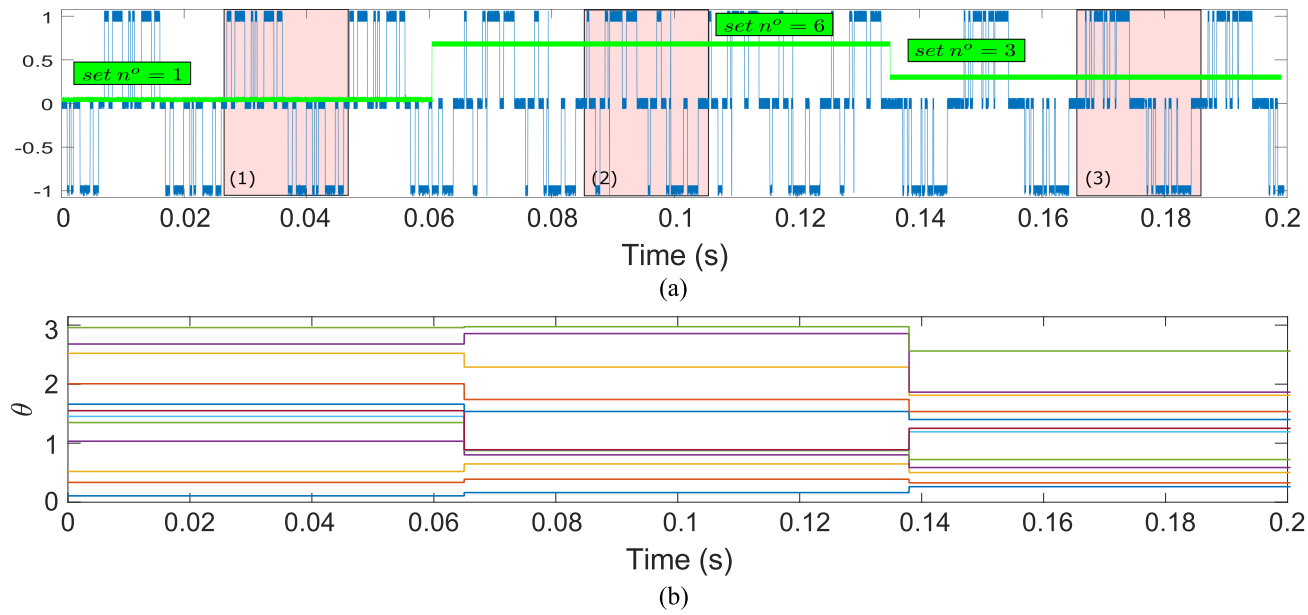

Fig. 17. (a) V_{a0} waveform for second case study. (1) $m_a = 0.7$, $m_5 = 0$, $\phi_5 = 0$. (2) $m_a = 0.7$, $m_5 = 0.45$, $\phi_5 = 1.6336$. (3) $m_a = 0.9$, $m_5 = 0.25$, $\phi_5 = \frac{\pi}{2}$. (b) Firing angles for second case study.

result, the harmonic content is presented in Figs. 18–20. The harmonics that have been regulated are highlighted in green, the triplen harmonics in red, and the rest in blue. As a three-phase system is used, the triplen harmonics are automatically eliminated in phase to phase voltages.

Fig. 18 represents the harmonic amplitudes when a sweep for different values of m_a (see Table I) is carried out for both case studies. The phase is not illustrated since ϕ_5 remains constant. In the first case, the values of m_5 and ϕ_5 are settled to 0.05 p.u. and 0 rd, respectively, and in the second case, to 0.15 p.u. and -1.1310 rd. Here, it can be clearly seen that the fundamental component follows the desired value for all the analyzed values.

The harmonic amplitudes when the sweep in m_5 (see Table I) is done are depicted in Fig. 19. In these cases, m_a and ϕ_5 values have been considered to be constant, being 0.9 pu and $\frac{\pi}{2}$ rd for the first case study and 0.7 p.u. and $-\frac{\pi}{2}$ rd for the second one. As it can be observed, for both cases, m_5 follows its reference value for all the swept values. In the second study case, there

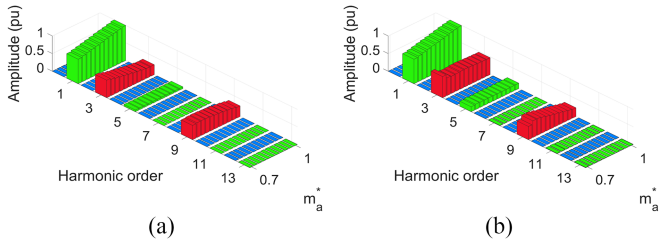

Fig. 18. Sweep in m_a. (a) Case study 1: $m_5 = 0.05$ and $\phi_5 = 0$. (b) Case study 2: $m_5 = 0.15$ and $\phi_5 = -1.1310$.

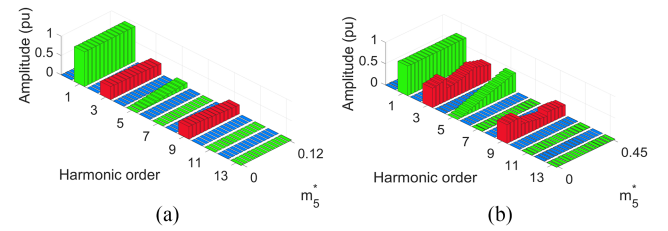

Fig. 19. Sweep in m_5. (a) Case study 1: $m_a = 0.9$ and $\phi_5 = \frac{\pi}{2}$. (b) Case study 2: $m_a = 0.7$ and $\phi_5 = -\frac{\pi}{2}$.

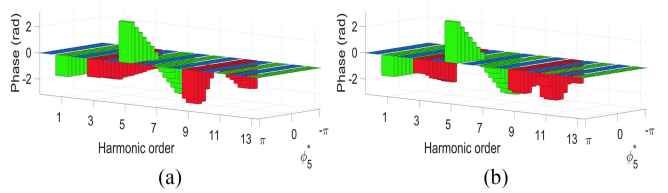

Fig. 20. Sweep in ϕ_5. (a) Case study 1: $m_a = 1.0$ and $m_5 = 0.12$. (b) Case study 2: $m_a = 0.8$ and $m_5 = 0.25$.

are two changes in the *set* n^o when m_5^* has a value of 0.12 and 0.33. This is appreciated in the triplen harmonics, which have a sudden change in their amplitude [Fig. 19(b)].

Finally, a sweep for the ϕ_5 variable (see Table I) is done. For the first case study $m_a = 1.0$ p.u. and $m_5 = 0.12$ p.u.; and, for the second case study, $m_a = 0.8$ p.u. and $m_5 = 0.25$ p.u. are selected. The obtained results are represented in Fig. 20, where the phase for each harmonic is shown. The generated 1st and 5th harmonic amplitudes are constant and the generated 5th harmonic phase perfectly follows the set-point. For the second case study, two different sets of switching angles have been used during the sweep.

In all the experimental tests carried out, it is observed that the fundamental harmonic amplitude and the 5th harmonic amplitude and phase are properly generated to different values. Consequently, it can be concluded that the proposed methodology and its implementation using ANNs provide optimal results, achieving a balance between time of response (required for RT applications) and accuracy of the proposed switching angles.

B. Execution Time Analysis

In Figs. 21 and 22, the probability of the execution time needed in RT for each case study, respectively, is plotted.

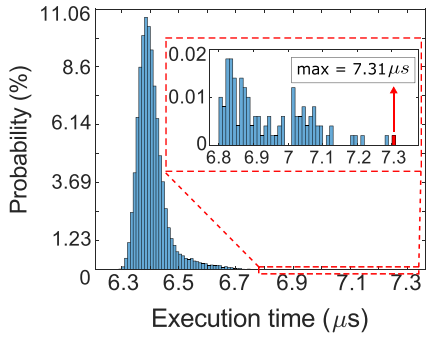

Fig. 21. Probability of execution time for case study 1.

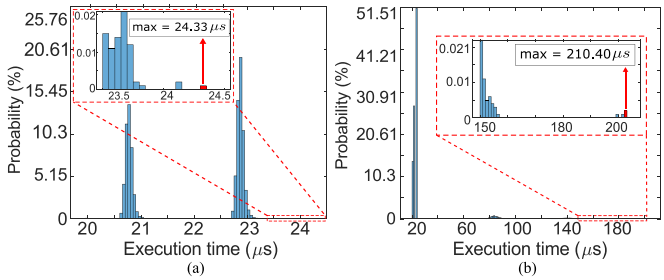

Fig. 22. Probability of execution time for case study 2. (a) Execution time using ANN. (b) Execution time using ANN and SQP.

This data is obtained as the mean time of ten executions for each (m_a, m_5, ϕ_5) combination. A maximum execution time of 300 μs is considered as a realistic modulation execution time of a high-power multilevel inverter [28].

Fig. 21 represents the time analysis for the first case study, where the mean execution time is 6.41 μs and the maximum time is 7.31 μs. This is due to the simplicity of the model, which only needs a single SA-ANN to approximate the switching angles.

The second case study has a higher complexity and a larger solution space compared to the first one. This needs two different ANNs to obtain the final switching angles: the classification ANN and the SA-ANN used to estimate the switching angles. Moreover, the size of these SA-ANN is larger, increasing the number of mathematical operations. Consequently, the mean and maximum execution time needed to run the ANNs have resulted higher, being 21.96 μs for the former and 24.33 μs for the latter, as depicted in Fig. 22(a).

As mentioned in Section V-B, for the second case study, using only the ANNs the (6) threshold for all the considered operating points is not satisfied. Therefore, the ANNs are hybridized with the SQP method. The number of iterations and number of executions per iteration of the SQP are critical factors that impact the overall execution time and quality. In order to limit the execution time, the maximum number of iterations and evaluations are set experimentally to 4 and 15, respectively. This means that the SA-ANN needs to estimate the switching angles as close as possible to the optimal values. Thus, the SQP method can converge to a valid solution in the defined number of executions using its exploitation ability. The probability of the execution

TABLE VI
DIFFERENT FPGA UTILIZATION FOR THE PROPOSED ANNS

FPGA model	LUT used	LUT available	Utilization (%)
Xc7z045ffg900-2	697	218 600	0.32
Xc7020clg484-1	695	53 200	1.31
Xc7z010clg225-3	883	17 600	5.02

time for each (m_a, m_5, ϕ_5) combination considering the hybrid ANN-SQP approach is depicted in Fig. 22(b). The mean and maximum times have resulted in $27.67\,\mu$s and $210.40\,\mu$s, respectively. This means that, for some operating points, the switching angles approximated by the ANNs are far from the valid solution, being necessary the use of the SQP. Favorably, they are close enough for the SQP to converge within the required maximum execution time.

Additionally, an augmented Lagrangian (AL) algorithm has also been tested in the proposed SHC-PWM modulator, instead of SQP, with the aim of improving the execution time. Specifically, a GHNN implements the AL algorithm [12]. This algorithm has been tested in the case study 2. As a result, a maximum execution time of $77\,\mu$s has been obtained in Speedgoat RT machine's Intel Core i7, reducing significantly the SQP computational cost. In addition, if the ANNs were executed in a FPGA, instead of in the CPU, the required CPU execution time would be reduced to $53\,\mu$s. In this way, processors with lower processing capacity than the Intel Core i7 used in experiments, such as the ARM dual-core Cortex-A9 embedded in the Zynq-7000 family recently used in power converters [32], [33], [34], could afford the online execution of the proposed SHC-PWM modulator with control frequencies commonly used in high-power applications. Moreover, to demonstrate the feasibility in terms of hardware requirements and consumed area in FPGA, the ANNs have been implemented in three different FPGAs of different capacities. Please note that the required ANNs are relatively simple (low number of layers and neurons per layer) compared to those used in other applications. Consequently, the utilization percentage needed in the three implementations is small as it can be observed in Table VI, needing a 5.02% of utilization in the worst case.

Therefore, as a result, the proposed approach fits the time requirements imposed, and thus, it is suitable for RT implementation.

IX. CONCLUSION

In this article, an SHC-PWM implementation based on ANNs for RT applications has been proposed. Here, the target is to synthesize not only a desired fundamental component, but also regulate the amplitude and phase of a single low-order harmonic, while eliminating other low-order harmonics. In order to achieve this, first an offline process is carried out where the solution space is calculated and the ANNs are trained, and afterwards, the trained ANNs are implemented online for RT execution.

A methodology that uses a hybridized metaheuristic-numerical offline search algorithm is used to calculate the switching angles. This methodology proposes some indicators to choose valid switching angles together with the steps to fill the solution space, trying to calculate the minimum number of sets of switching angles. In case where more than one set of firing angles is needed, an hysteresis between the sets of switching angles is ensured, minimizing the number of transitions between sets and, consequently, overcurrent problems.

The obtained sets of switching angles are used to train offline a set of ANNs that estimate in RT the switching angles without using LUTs, making the simultaneous regulation of several harmonics affordable, as it is required by applications such as APFs. The use of ANNs reduce significantly the storage requirements, with respect to the use of LUTs, when the number of harmonics to be controlled increases. The proposed approach has been experimentally validated for a 3 L converter when m_a, m_5, and ϕ_5 are regulated and the 7th, 11th, and 13th harmonics are eliminated.

Two different case studies have been analyzed: 1) a solution space covered using a single set of switching angles; and 2) another solution space that needs multiple sets of switching angles to be filled. For the first case study just one SA-ANN is required to calculate the final switching angles. For the second case study, a classification ANN is needed to first decide which SA-ANN (a different SA-ANN has been trained for every existing set) is executed. As the solution space is complex, the SA-ANN might not provide enough accuracy in some operating points. Thus, in those cases, its output is refined with an SQP algorithm.

The ANNs have been executed in a RT target machine in order to verify their correct performance and the validity of the proposed 3-D search methodology. The results obtained for both case studies show that the proposed method is able to regulate m_a, m_5, and ϕ_5 to their desired reference values. Additionally, for the second case study, the classification ANN works correctly, activating different SA-ANN depending on the operating point. It has been verified that the hybridization of the ANNs with an SQP method is necessary to fulfill the (6) threshold for all the operating points. Regarding the execution time, this depends on the solution space complexity, the number of ANNs used along with their size, and the required SQP execution. For both case studies, the execution time constraint has been satisfied. Additionally, the SHC-PWM execution time has been further improved replacing SQP with the AL algorithm. All these analyses validate the proposed SHC-PWM modulator based on ANN for RT applications. This modulator can be extended to any number of switching angles and converter levels.

The main challenge of the modulator is the computational time required for offline calculation of the solution space. Future work will focus on reducing this time, enabling regulation of a higher number of harmonics simultaneously. Furthermore, the closed-loop control is an interesting area to be analyzed, which can be built upon this proposal.

REFERENCES

[1] J. I. Leon, S. Vazquez, and L. G. Franquelo, "Multilevel converters: Control and modulation techniques for their operation and industrial applications," *Proc. IEEE*, vol. 105, no. 11, pp. 2066–2081, Nov. 2017.

[2] J. Rodriguez, S. Bernet, B. Wu, J. O. Pontt, and S. Kouro, "Multilevel voltage-source-converter topologies for industrial medium-voltage drives," *IEEE Trans. Ind. Electron.*, vol. 54, no. 6, pp. 2930–2945, Dec. 2007.

[3] S. Kouro et al., "Recent advances and industrial applications of multilevel converters," *IEEE Trans. Ind. Electron.*, vol. 57, no. 8, pp. 2553–2580, Aug. 2010.
[4] M. S. A. Dahidah, G. Konstantinou, and V. G. Agelidis, "A review of multilevel selective harmonic elimination PWM: Formulations, solving algorithms, implementation and applications," *IEEE Trans. Power Electron.*, vol. 30, no. 8, pp. 4091–4106, Aug. 2015.
[5] L. G. Franquelo, J. Napoles, R. C. P. Guisado, J. I. Leon, and M. A. Aguirre, "A flexible selective harmonic mitigation technique to meet grid codes in three-level PWM converters," *IEEE Trans. Ind. Electron.*, vol. 54, no. 6, pp. 3022–3029, Dec. 2007.
[6] R. P. Aguilera et al., "Selective harmonic elimination model predictive control for multilevel power converters," *IEEE Trans. Power Electron.*, vol. 32, no. 3, pp. 2416–2426, Mar. 2017.
[7] A. Pérez-Basante, S. Ceballos, G. Konstantinou, J. Pou, I. Kortabarria, and I. M. D. Alegría, "A universal formulation for multilevel selective-harmonic-eliminated PWM with half-wave symmetry," *IEEE Trans. Power Electron.*, vol. 34, no. 1, pp. 943–957, Jan. 2019.
[8] J. Hao, G. Zhang, Y. Zheng, W. Hu, and K. Yang, "Solution for selective harmonic elimination in asymmetric multilevel inverter based on stochastic configuration network and levenberg-marquardt algorithm," in *Proc. IEEE Appl. Power Electron. Conf. Expo.*, 2019, pp. 2855–2858.
[9] S. Padmanaban, C. Dhanamjayulu, and B. Khan, "Artificial neural network and newton raphson (ANN-NR) algorithm based selective harmonic elimination in cascaded multilevel inverter for PV applications," *IEEE Access*, vol. 9, pp. 75058–75070, 2021.
[10] I. Khoukha, C. Hachemi, and B. El Madjid, "Ann control of nine level NPC voltage inverter based on selective harmonics elimination," in *Proc. Int. Aegean Conf. Elect. Machines Power Electron.*, 2007, pp. 587–591.
[11] K. Yang, J. Hao, and Y. Wang, "Switching angles generation for selective harmonic elimination by using artificial neural networks and quasi-newton algorithm," in *Proc. IEEE Energy Convers. Congr. Expo.*, pp. 1–5, 2016.
[12] M. Balasubramonian and V. Rajamani, "Design andreal-time implementation of SHEPWM in single-phase inverter using generalized hopfield neural network," *IEEE Trans. Ind. Electron.*, vol. 61, no. 11, pp. 6327–6336, Nov. 2014.
[13] K. Yang et al., "Real-time switching angle computation for selective harmonic control," *IEEE Trans. Power Electron.*, vol. 34, no. 8, pp. 8201–8212, Aug. 2019.
[14] P. Enjeti and J. F. Lindsay, "Solving nonlinear equations of harmonic elimination PWM in power control," *Electron. Lett.*, vol. 23, pp. 656–657, Jun. 1987.
[15] R. Pindado, C. Jaen, and J. Pou, "Robust method for optimal PWM harmonic elimination based on the chebyshev functions," in *Proc. 8th Int. Conf. Harmon. Qual. Power.*, pp. 976–981, 1998.
[16] J. N. Chiasson, L. M. Tolbert, K. J. McKenzie, and Z. Du, "Elimination of harmonics in a multilevel converter using the theory of symmetric polynomials and resultants," *IEEE Trans. Control Syst. Technol.*, vol. 13, no. 2, pp. 216–223, Mar. 2005.
[17] K. Yang, Z. Yuan, R. Yuan, W. Yu, J. Yuan, and J. Wang, "A groebner bases theory-based method for selective harmonic elimination," *IEEE Trans. Power Electron.*, vol. 30, no. 12, pp. 6581–6592, Dec. 2015.
[18] M. A. Memon, M. D. Siddique, S. Mekhilef, and M. Mubin, "Asynchronous particle swarm optimization-genetic algorithm (APSO-GA) based selective harmonic elimination in a cascaded H-bridge multilevel inverter," *IEEE Trans. Ind. Electron.*, vol. 69, no. 2, pp. 1477–1487, Feb. 2022.
[19] S. Ahmad, M. Al-Hitmi, A. Iqbal, K. Rahman, and I. Ashraf, "Low switching frequency modulation of a 3 x 3 matrix converter in upfc application using differential evolution method," *Int. Trans. Elect. Energy Syst.*, vol. 30, 2019, Art. no. e12179.
[20] I. Ibanez-Hidalgo et al., "Methodology to compare meta-heuristic algorithms to solve selective harmonic elimination-PWM and optimal pulse pattern formulations," in *Proc. 47th Annu. Conf. IEEE Ind. Electron. Soc.*, 2021, pp. 1–6.
[21] F. Filho, H. Z. Maia, T. H. A. Mateus, B. Ozpineci, L. M. Tolbert, and J. O. P. Pinto, "Adaptive selective harmonic minimization based on ANNs for cascade multilevel inverters with varying DC sources," *IEEE Trans. Ind. Electron.*, vol. 60, no. 5, pp. 1955–1962, May 2013.
[22] A. Janabi, B. Wang, and D. Czarkowski, "Generalized chudnovsky algorithm for real-time PWM selective harmonic elimination/modulation: Two-level VSI example," *IEEE Trans. Power Electron.*, vol. 35, no. 5, pp. 5437–5446, May 2020.
[23] P. Farhadi, M. Navidi, M. Gheydi, M. Pazhoohesh, and H. Bevrani, "Online selective harmonic minimization for cascaded half-bridge multilevel inverter using artificial neural network," in *Proc. Int. Aegean Conf. Elect. Mach. Power Electron. Int. Conf. Optim. Elect. Electron. Equip., Int. Symp. Adv. Electromechanical Motion Syst.*, 2015, pp. 331–335.
[24] M. Manoharsha, B. Babu, K. Veeresham, and R. Kapoor, "ANN based selective harmonic elimination for cascaded h-brdige multilevel inverter," in *Proc. 7th Int. Conf. Elect. Energy Syst.*, 2021, pp. 183–188.
[25] M. Banaei and P. Shayan, "Solution for selective harmonic optimisation in diode-clamped inverters using radial basis function neural networks," *Power Electron. IET*, vol. 7, pp. 1797–1804, 2014.
[26] G. Amar, C. Larbes, D. Bendib, L. Hassaine, and A. Malek, "FPGA based on-line artificial neural network selective harmonic elimination PWM technique," *Int. J. Elect. Power Energy Syst.*, vol. 68, pp. 33–43, 2015.
[27] A. Moeini, M. Dabbaghjamanesh, T. Dragičević, J. W. Kimball, and J. Zhang, "Chapter 6 - Machine learning technique for low-frequency modulation techniques in power converters," *Frede Blaabjerg, Control of Power Electronic Converters and Systems*. Cambridge, MA, USA: Academic Press, 2021, pp. 149–167.
[28] H. Fernandez-Rebolleda et al., "Analysis and optimization of modulation transitions in medium-voltage high-power converters," *IEEE Trans. Power Electron.*, vol. 36, no. 9, pp. 9984–9993, Sep. 2021.
[29] I. Ibanez-Hidalgo et al., "Error tolerance analysis for she-PWM calculation in a 3l-NPC converter," in 2021*Proc. 47th Annu. Conf. IEEE Ind. Electron. Soc.*, 2021, pp. 1–8.
[30] S. J. W. Jorge Nocedal, *Numerical Optimization*. 2nd ed. Berlin, Germany: Springer, 2006.
[31] A. Jain, J. Mao, and K. Mohiuddin, "Artificial neural networks: A tutorial," *Computer*, vol. 29, pp. 31–44, Mar. 1996.
[32] F. Rojas-Rocco, C. Baier-Fuentes, R. Ramírez-Alegría, M. Díaz-Bustos, and P. Melin-Coloma, "Application of the zynq 7000 system in the control of a boost converter," in *Proc. IEEE Chilean Conf. Elect. Electron. Eng. Inf. Commun. Technol.*, 2019, pp. 1–6.
[33] C. Buccella, C. Cecati, and H. Latafat, "Digital control of power converters–a survey," *IEEE Trans. Ind. Informat.*, vol. 8, no. 3, pp. 437–447, Aug. 2012.
[34] T. Heath et al., "Cascaded- and modular-multilevel converter laboratory test system options: A review," *IEEE Access*, vol. 9, pp. 44718–44737, 2021.

Irati Ibanez-Hidalgo (Graduate Student Member, IEEE) received the B.Sc. and the M.Sc. degrees in industrial engineering from the University of the Basque Country (UPV/EHU), Bilbao, Spain, in 2018 and 2020, respectively. She is currently working toward the Ph.D. degree with the Tecnalia Research and Innovation on the implementation in real time of low-frequency modulation techniques for high-power converters.

Since 2020, she has been with the Department of Systems Engineering and Automation, University of the Basque Country (UPV/EHU), researching in the area of power electronics in collaboration with Tecnalia Research and Innovation, Derio, Spain, and Ingeteam R&D Europe, Zamudio, Spain. From 2022 to 2023, she was a Visiting Researcher with the University of Technology Sydney, Sydney, Australia. Her research interests include active power filters, modulation and control of power converters, multilevel converters, and low-frequency modulation techniques.

Alain Sanchez-Ruiz (Senior Member, IEEE) received the B.Sc. degree in electronics engineering, the M.Sc. degree in automatics and industrial electronics, and the Ph.D. degree in electrical engineering from the University of Mondragon, Mondragon, Spain, in 2006, 2009, and 2014, respectively.

From February 2012 to May 2012, he was a Visiting Researcher with the University of Tennessee, Knoxville, TN, USA. From 2014 to 2022, he was an R&D Engineer with Ingeteam R&D Europe, Zamudio, Spain. Since 2017, he has been an Assistant Professor with the University of the Basque Country (UPV/EHU), Vitoria-Gasteiz, Spain. His current research interests include modeling, modulation and control of power converters, multilevel topologies, advanced modulation techniques, high-power converters, grid-tied converters, renewable energy, and green hydrogen systems.

Dr. Sanchez-Ruiz is an Associate Editor for IEEE TRANSACTIONS ON INDUSTRIAL ELECTRONICS.

Angel Perez-Basante received the B.Eng. degree in telecommunications engineering from the University of Valladolid, Valladolid, Spain, in 2006, the M.Eng. degree in electronic systems engineering from the Technical University of Madrid (UPM), Madrid, Spain, in 2012, and the Ph.D. degree in advanced electronic systems engineering from the University of the Basque Country (UPV/EHU), Bilbao, Spain, in 2017. From 2012 to 2016, he was working toward the Ph.D. degree with the Applied Electronics Research Team (APERT), University of the Basque Country (UPV/EHU) in collaboration with Tecnalia Research and Innovation, Derio, Spain. He is currently working as a researcher with Tecnalia Research and Innovation and his main research interest include multilevel converters, advance modulation and control strategies, and stability analysis of electrical systems.

From September 2015 to December 2015, he was a Visiting Researcher with the Chair of Power Electronics, Christian Albrechts University, Kiel, Germany. Since 2017, he is a Researcher with the Energy, Climate and Urban Transition Unit, Tecnalia Research and Innovation. His main research interests include multilevel converters, advanced modulation and control strategies, and stability analysis of electrical systems.

Asier Zubizarreta received the Ph.D. degree in robotics and automatic control systems from the University of the Basque Country (UPV/EHU), Bilbao, Spain, in 2010.

He is currently an Associate Professor with the Department of Automatic Control and Systems Engineering, Faculty of Engineering, UPV/EHU. He is currently focused on the development of artificial intelligence-based virtual sensors for complex applications such as those in the field of power electronics, biomedical engineering, or smart manufacturing. In addition, he works in the application of model-based predictive control approaches for high dynamic systems, such as power electronics and automated driving.

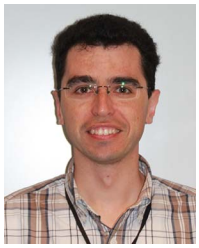

Salvador Ceballos received the M.S. degree in physics from the University of Cantabria, Santander, Spain, in 2001, and the M.S. and Ph.D. degrees in electronic engineering from the University of the Basque Country, Bilbao, Spain, in 2002 and 2008, respectively.

Since 2002 he has been a Principal Researcher with the Energy, Climate and Urban Transition Unit, Tecnalia Research and Innovation, Derio, Spain. His research interests include multilevel converters for high and medium voltage applications, fault-tolerant power electronic topologies, renewable energy systems, and power systems with high penetration of power converters.

Sergio Gil-Lopez received the M.Sc. degree in physics from Universidad de La Laguna, Tenerife, Spain, in 2001, and the Ph.D. degree in atmospheric physics from IAA, CSIC, Universidad de Granada, Granada, Spain, in 2006.

During his Ph.D. studies, he spent three months with two Atmospheric German Researcher centers for scientist collaboration. He has authored or coauthored more than 40 international journal papers and more than 43 conference contributions, 7 filed patents, and has supervised 2 Ph.D.s. He is currently the head of the AI group of Tecnalia Research and Innovation, Derio, Spain, where he is also a Data Scientist Senior Researcher with more than 15 years of experience. He was also with Ariadna Instrument S. L., Biscay, Spain, working in the developing of an intelligent algorithm for low voltage network topology estimation, fraud detection techniques, and energy balance estimations for the smart grids. His research interests include tackling smart analytics applied to energy optimization, smart grids, or Industry4.0.

Dr. Gil-Lopez was the recipient of the DataSciAwards 2019 in the category Best Use of Data Science/AI for Industry 4.0 and Winner of the Advanced Factory Awards 2020 in the Category of "Research and development of artificial intelligence applied in industrial plants."

Ricardo P. Aguilera (Member, IEEE) received the B.Sc. degree in electrical engineering from Universidad de Antofagasta, Antofagasta, Chile, in 2003, the M.Sc. degree in electronics engineering from the Universidad Tecnica Federico Santa Maria, Valparaíso, Chile, in 2007, and the Ph.D. degree in electrical engineering from The University of Newcastle (UoN), Newcastle, NSW, Australia, in 2012.

From 2012 to 2013, he was a Research Academic with UoN, where he was part of the Centre for Complex Dynamic Systems and Control. From 2014 to 2016, he was a Senior Research Associate with The University of New South Wales, Australia, where he was part of the Australian Energy Research Institute. Since September 2016, he has been an Associate Professor with the School of Electrical and Data Engineering, University of Technology Sydney, Sydney, Australia. His main research interests include theoretical and practical aspects on model predictive control with application to power electronics, renewable energy integration, and microgrids.